Machinery & Energetics
Vol. 14, No. 3. 2023

Journal homepage:
https://technicalscience.com.ua/en

UDC 621.313.33:621.318.122
DOI: 10.31548/machinery/3.2023.34

Stefan Junge[*]
Doctor of Technical Sciences, Professor
Berlin University of Applied Sciences
13353, 10 Luxemburger Str., Berlin, Germany
https://orcid.org/0000-0002-8045-4103

Nikolay Zablodskiy[*]
Doctor of Technical Sciences, Professor
National University of Life and Environmental Sciences of Ukraine
03041, 15 Heroiv Oborony Str., Kyiv, Ukraine
https://orcid.org/0000-0001-8889-8158

Natalya Zaiets
Doctor of Technical Sciences, Professor
National University of Life and Environmental Sciences of Ukraine
03041, 15 Heroiv Oborony Str., Kyiv, Ukraine
https://orcid.org/0000-0001-5219-2081

Roman Chuenk
PhD in Technical Sciences, Associate Professor
National University of Life and Environmental Sciences of Ukraine
03041, 15 Heroiv Oborony Str., Kyiv, Ukraine
https://orcid.org/0000-0002-9339-9764

Stanislav Kovalchuk
Postgraduate Student
National University of Life and Environmental Sciences of Ukraine
03041, 15 Heroiv Oborony Str., Kyiv, Ukraine
https://orcid.org/0000-0002-1194-3464

The screw-type electrothermomechanical converter as a source of multiphysical influence on the technological environment

Abstract. In ensuring the reliability of electromechanical converters in harsh conditions, the problem of increasing the energy efficiency of their application through structural, functional, and thermal integration with the technological environment is present. Thus, the research aims to determine the conditions of the direct multiphysical impact of a screw-type electromechanical converter on the technological environment. The method used is based on determining the list of features of screw-type electromechanical converters using the Comsol Multiphysics software, and a combination of three-dimensional and two-dimensional finite element models limited to the rotor with the inclusion of blades in the computational domain. Two variants of forming an algorithm for the multiphysical impact on the technological environment were studied: local concentration of the impact in certain areas of the rotor and uniform distribution along the rotor surface of temperature, pressure, magnetic induction, and electric field strength. The regularities of the distribution of magnetic

Article's History: Received: 03.04.2023; Revised: 12.07.2023; Accepted: 11.08.2023.

Suggested Citation:
Junge, S., Zablodskiy, N., Zaiets, N., Chuenko, R., & Kovalchuk, S. (2023). The screw-type electrothermomechanical converter as a source of multiphysical influence on the technological environment. *Machinery & Energetics,* 14(3), 34-46. doi: 10.31548/machinery/3.2023.34.

*Corresponding author

induction on the outer surface of the ferromagnetic rotor at different azimuthal locations of the frontal parts of adjacent stators have been established. The distribution of the normal component of the magnetic flux density at the contact with the process medium in the form of rutile product or ilmenite concentrate is determined. The consumed electric energy is distributed in the stator tooth zone and the zone of electromagnetic field penetration into the rotor. Eddy currents are concentrated at the penetration depth from the rotor's inner surface, with the penetration depth depending on the thermal state and sliding mode. The electric field intensity on the rotor's outer surface reaches 0.8 V/m in the areas opposite the stator crowns and depends on the current activity of the phases at a given moment. Controlling the thermal and speed regime of the rotor can be used to create conditions for bioenergy stimulation on its surface in places of contact with the medium or to support the process of electrode heating of the technological medium. The adequacy of the mathematical models proposed for numerical modelling to the experimental data of the prototype of the screw electromechanical converter was confirmed, with deviations not exceeding 9.5%. The obtained results can be used to predict the optimal indicators of electromagnetic and heat transfer processes in screw electromechanical converters associated with the technological environment

Keywords: magnetic induction; eddy currents; temperature field; electromagnetic field; thermogram, magnetic permeability

INTRODUCTION

Most electromagnetic devices (EMDs) are characterised by the simultaneous action of electromagnetic, thermal, vibration, mechanical and acoustic fields not only on the electromagnetic core of the device but also on the technological environment. These EMDs contain continuously moving or stationary parts with the required electrical conductivity and magnetic properties that are in direct contact with the process medium - solid, liquid, gaseous and multiphase objects that are actively or passively used in the technological process of production or use of products. An urgent problem is the drying and processing of wet dispersed waste from food production, which can then be effectively used as fertiliser, livestock feed or biofuel (Bulgakov *et al.*, 2020).

A special category of EMDs is represented by solid rotor induction motors (SRIMs), which, due to their rigid construction and integrity, can operate at the highest required rotational speeds. These machines can be used in aggressive and humid environments and integrate design and functionality with the process. All types of energy dissipation in such machines are used to process raw materials. For example, in screw electromechanical converters (SEMCs), an external massive rotor can contact the processing medium and create multiphysical processes for processing raw materials (Zablodskiy *et al.*, 2021).

T. Wolnik & T. Jarek (2022) compared the losses, power factors, and efficiency of induction motors with a solid and shielded rotor magnetic circuit. It was found that the increase in total losses of the solid rotor is primarily due to the growth of eddy current losses in the presence of higher harmonics and subharmonics in the magnetic flux harmonic spectrum. The comparison of design parameters and weight reveals that the solid rotor has a simplified design and manufacturing technology and a lower weight, especially for motors with an external rotor.

To increase the power factor, V. Kaplun *et al.* (2022) suggested using internal capacitive compensation of the reactive power of an induction motor. A winding with two parallel windings in each phase is used, one of which forms the main winding that is connected to the power supply network. The other parallel winding in the core slots is offset relative to the main winding and forms an additional winding that is switched on according to the scheme of a rotary autotransformer to an electric capacitance. A comparison of the modelling results of the basic and improved motors indicates the possibility of increasing energy efficiency and torque when using internal capacitive reactive power compensation.

C.A. Wengerkievicz *et al.* (2022) analysed the possibilities of determining the loss distribution of an induction machine with a two-phase stator winding and a massive groove-less rotor by testing according to standard methods used for squirrel-cage induction motors. Even if a high operating frequency is required, the tests are carried out at a reduced frequency and voltage to avoid the influence of time harmonics. It is proposed to adjust the loss distribution to take into account the effect of high slip without load, as well as to analyse parasitic losses during load tests. The final test results are extrapolated to establish nominal conditions. According to C. Mellak *et al.* (2022), motors with a solid rotor have higher mechanical and thermal stability, and better stator current to electromagnetic torque ratio at high slip, which makes them suitable for compressor production, railway electric transport, and medicine.

However, there are applications where efficiency may not be the most important parameter. In this case, the technological environment may have high temperature, pressure and humidity or a limited volume. To predict losses, A. Laidoudi *et al.* (2020) proposed an analytical model that is combined with a thermal model to predict the temperature in different parts of the machine and the effect of temperature on parameters important for EMD performance.

A wide range of technological processes with heavy temperature loads exist that require the direct coupling of rotating parts of EMDs with actuators. M.M. Mazlan *et al.* (2019), and F. Campuzano *et al.* (2019) proved the effectiveness of using a screw converter in the processing of bulk and plastic substances. The influence of hydrolysis parameters on the mixing torque was investigated for single- and twin-screw electromechanical converters by C. Feng *et al.* (2019). In these studies, regression models were developed to establish a correlation between system parameters and time-varying parameters. M. Mushtruk *et al.* (2020) investigated the issue of high energy consumption associated with machining in an electromechanical screw converter.

A feature of the considered methods and results of studies of electromechanical converters is the stationary temperature conditions of the surrounding cooling medium. However, for screw-type electromechanical converters (SEMCs) for technological purposes, studies with nonlinear changes in the load-cooling medium become relevant. The second important feature of the design and application conditions of the SEMC is that the presence of a wide range of harmonics in the distribution of its resulting magnetic field, which forms eddy current losses, is a useful component for ensuring the temperature regime in the rotor-technological environment system. At the same time, the electromagnetic system of the SEMC should provide the required electromechanical characteristics and overall efficiency. As such, along with solving the problem of ensuring the reliability of electromechanical converters in harsh environments, a scientific demand for improving the energy efficiency of their use through structural, functional, and thermal integration with the technological environment is present. Thus, the research aims to determine the conditions of the direct multiphysical influence of an electromechanical screw-type converter on the technological environment.

MATERIALS AND METHODS

The research was carried out at the Educational and Research Institute of Energy, Automation and Energy Saving of the National University of Life and Environmental Sciences of Ukraine in 2020-2022. The object of the study was electromagnetic, electromechanical, and thermal processes in the electromagnetic system of the screw electromechanical converter (SEMC) and the areas of direct contact of the external massive rotor screw with the technological environment. Two variants of forming an algorithm for the multiphysical influence on the technological environment in accordance with the technological process were considered: the first variant is the local concentration of such impact in certain areas of the rotor; the second variant is the uniform distribution along the rotor surface of temperature, pressure, magnetic induction, and electric field intensity. Numerical modelling was carried out for the SEMC, a fragment of the electromagnetic system design which is shown in Figure 1.

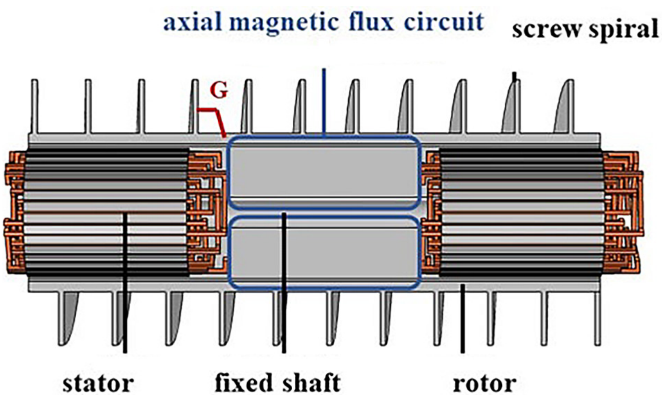

Figure 1. The SEMC electromagnetic system

Note: blue contours show the circulation of the longitudinal magnetic flux in the intermodule zone; G – outer surface of the rotor with the rotor helical blades (ribs)

Source: compiled by the authors

A method based on the numerical determination of the characteristics of the SEMC using a combination of three-dimensional and two-dimensional finite element models, limited by the rotor with the inclusion of blades in the computational domain is applied. Considering the identity of electromagnetic and thermal processes occurring on the stator-common rotor modules of the electromagnetic system of the SEMC, the simulation was carried out for one of them in the Comsol Multiphysics software environment (AC/DC Module User's Guide, COMSOL Inc., Burlington, MA, USA, 2018). The numerical analysis of the electromagnetic field was carried out using a mathematical model (MM) and the spatial distribution of the grid of an electromechanical screw-type device for the hydrolysis processing of feathers (Fig. 2).

The operating loading and cooling medium are in direct contact with the screw rotor. Depending on the loading mode of the SEMC, the process medium can be represented in the following types: at idle (system warm-up mode) - air; at the main operating mode - a continuous heterogeneous medium using averaged characteristics (specific conductivity, magnetic and dielectric constant).

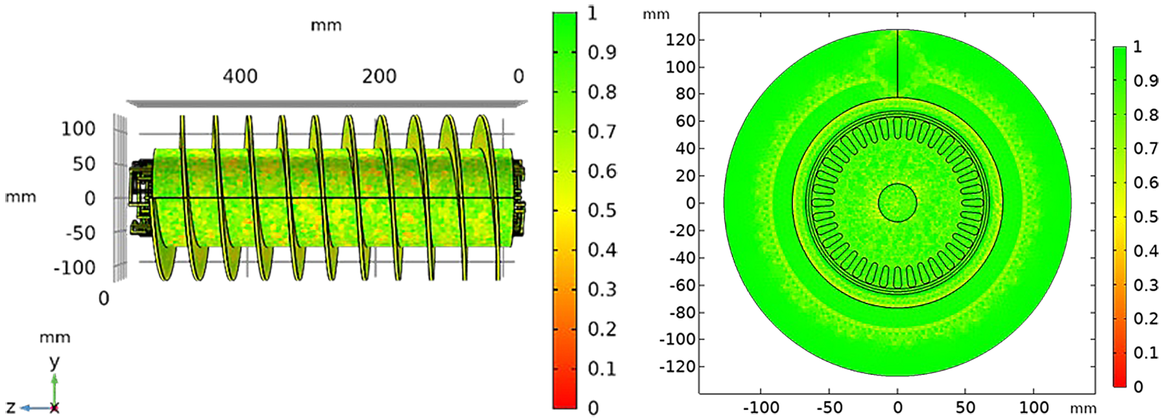

Figure 2. Finite element mesh in the design domain
Source: N. Zablodskiy *et al.* (2021)

Considering these properties of the technological environment, other vectors of electric induction and magnetic field strength were introduced to account for all the induced currents, namely: polarisation current of bound charges; free carrier current; eddy current of magnetisation:

$$D(r,t) = E(r,t) + 4\pi P(r,t);\ H(r,t) = B(r,t) + 4\pi M(r,t), \quad (1)$$

where $P(r,t) = \int_{-\infty}^{t} j(r,t)\, dt$ – a polarisation density vector that combines induced currents of all types; $M(r,t)$ – the magnetisation vector of the operating environment.

When modelling the main mode of operation of the SEMC, ilmenite and rutile with a specific electrical conductivity of $10^{-1} \leqslant \rho \leqslant 10_4$ S/m were considered as a heterogeneous medium surrounding the screw rotor, which differs in magnetic properties: ilmenite is weakly magnetic (specific magnetic susceptibility $24 \cdot 10^{-7}$ m^3/kg), and rutile is non-magnetic (specific magnetic susceptibility $0.25 \cdot 10^{-7}$/kg).

Considering the factor of the discrete location of the stators, an important stage of research was to determine the electromagnetic and thermal characteristics of the intermodule section of the rotor. For the second variant of forming an algorithm for the multiphysical impact on the technological environment, namely, the uniform distribution along the rotor surface of temperature, pressure, magnetic induction, and electric field strength, a method based on the numerical determination of the transverse and longitudinal edge effect of a common rotor for two SEMC stators using a combination of three-dimensional and two-dimensional finite element models was proposed. These effects, by matching the magnetic fluxes of the frontal parts of adjacent stators, are used in the numerical model of the SEMC to ensure uniformity of the rotor temperature field in the intermodule zone and increase the energy performance of the SEMC.

The distribution of a plane electromagnetic wave in the intermodule zone during the passage of an alternating magnetic flux Φ_m along a steel rotor cylinder was considered (Fig. 1). Since the average diameter of the hollow cylindrical rotor of the screw SEMC is an order of magnitude greater than its thickness, and the rotor thickness b of the SEMC prototype exceeds the penetration depthΔ_{ew}, the influence of wave curvature and reflection can be neglected, and a flat electromagnetic field can be assumed to penetrate the rotor in the intermodule zone from both sides.

To verify the modelling results, two prototypes of the SEMC with different azimuthal arrangements of the fronts of adjacent stators were tested: the prototype – an arbitrary azimuthal arrangement of the fronts of adjacent stators; the second prototype - magnetic fluxes of the fronts of adjacent stators coordinated in space and time. The nominal data of the SEMC are power consumption P = 1900 W; supply voltage U = 80 V; current consumption I = 30 A; power factor cos φ = 0,65; number of poles – 6; rotation frequency n = 180 rpm. Figure 3 shows the components of the prototype SEMC with the definition of the zones for measuring electromagnetic and temperature parameters.

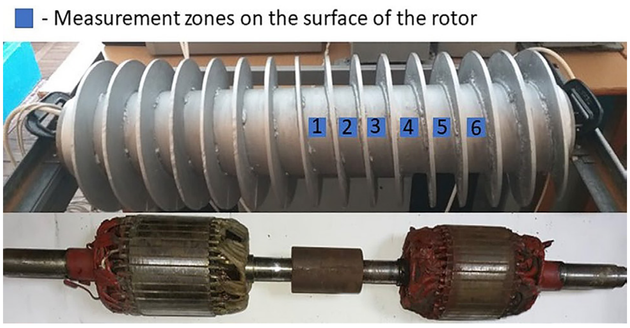

Figure 3. Distribution of measurement zones of electromagnetic and temperature parameters on the surface of the outer rotor of the mock-up sample of the SEMC
Note: the figure shows the corresponding arrangement of the system of adjacent stators placed in the outer rotor cavity
Source: compiled by the authors

Measurements of electromagnetic and temperature parameters on the prototypes were performed in short-circuit mode (braked rotor) with the supply voltage reduced to the level at which the rated current is achieved.

The following measuring devices were used in the empirical studies: Tenmars TM-191 Magnetic Field Meter (manufactured in Taiwan), designed to measure ultra-low frequency electromagnetic fields from 30 Hz to 300 Hz; Tenmars TM-190 Multi-Field EMF Meter (Taiwan) – a device for measuring high-frequency electromagnetic fields in the frequency range from 50 MHz to 3.5 GHz and low-frequency electric and magnetic fields in the frequency range of 50-60 Hz; infrared, optical pyrometer BENETECH GM533A (China), measuring range -50-530°C, visibility index 12: 1, thermal radiation coefficient 0.1-1, spectrum 5-14 μm; thermal imager Xintest HTI HT-18 (country of origin China), thermal sensitivity 0.07°C, temperature range: -20°C--300°C, image capture frequency 8 Hz, wavelength range 8-14 μm.

RESULTS AND DISCUSSION

The research methodology allowed us to establish a wide range of parameters and regularities through modelling and experimental measurements, but this section presents primarily the results of determining the conditions for the direct multiphysical influence of the screw-type electromechanical converter on the technological environment. Figure 4 shows the distribution of magnetic field induction in the stator plane of a separate SEMC module. The levels of magnetic induction in the stator tooth zone do not exceed 1.4 T, which indicates the absence of saturation zones and is explained by the low voltage value on the winding phases. The highest values of magnetic induction (up to 2.8 T) are observed on the side of the inner surface of the rotor at the depth of penetration Δ of the electromagnetic field into the rotor array. In the array and on the outer surface of the rotor, which is in direct contact with the process medium, 6 wide and 6 narrow zones are formed in a circular pattern alternating in a circle following the number of poles. On the outer surface, the magnetic field induction levels for the wide (opposite the poles) and narrow zones are 0.6 T and 0.1 T, respectively.

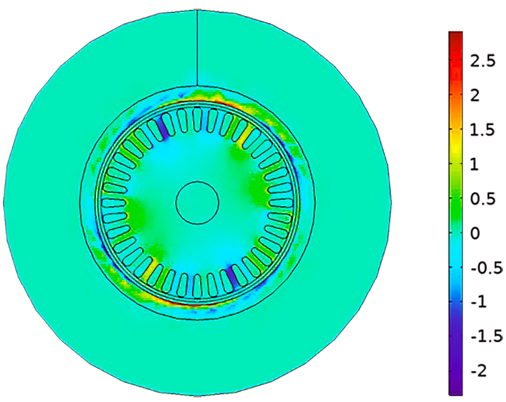

Figure 4. Induction of a magnetic field in the stator plane of a single module of an SEMC
Note: scale dimension – T
Source: compiled by the authors

The distribution of the normal component of the magnetic flux density of the SEMC coincides with the results of modelling electromechanical converters of the submersible type for oil production technologies in terms of the levels of magnetic induction in the stator tooth zone, on the inner and outer surfaces of the rotor, and at the depth of electromagnetic wave attenuation in the rotor ferromagnetic body (Zablodskiy *et al.*, 2014).

With an increase in the supply voltage, the magnetic flux penetrates much deeper into the rotor, as noted by C.A. Wengerkievicz *et al.* (2022), but in this case, the study concerns a massive hollow rotor with helical blades (fins) external to the stator. Since the array of the external solid rotor of the SEMC is simultaneously conductive for magnetic flux and eddy currents, the nature of the distribution of electromagnetic parameters in it differs significantly from induction machines with a shielded rotor.

Figure 5 shows the distribution of the normal component of the magnetic flux density for the cross-section of the SEMC module in the presence of contact with the process medium in the form of rutile product or ilmenite concentrate.

a)
b)

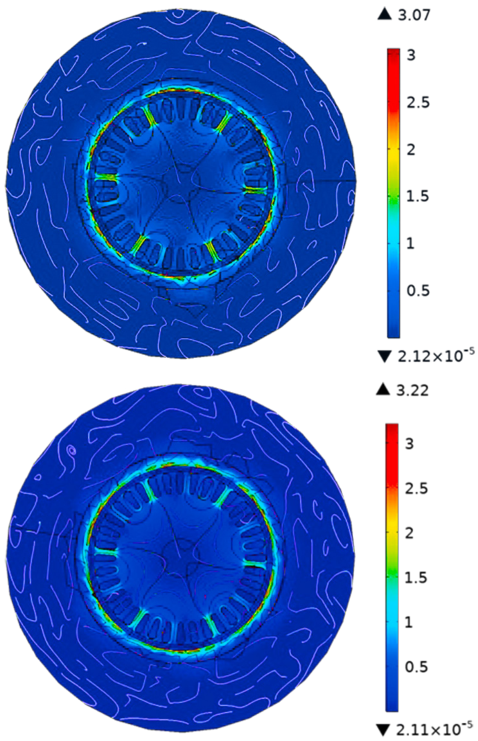

Figure 5. Magnetic flux density during SEMC operation
Note: scale dimension - T; a) – with rutile product; b) – with ilmenite concentrate
Source: compiled by the authors

Rutile product slightly weakens the external magnetic field in the rotor surface area and deviates from the rotor surface, while ilmenite concentrate, on the contrary, strengthens the magnetic field and adheres tightly to the rotor surface.

The SEMC can be used for heating up to 110°-120°C and transporting it to the production of commercial rutile concentrate, as well as preheating non-conductor industrial products before feeding them to an electrostatic separator to produce zircon product.

Figure 6 shows a three-dimensional image of the magnetic induction distribution on the outer surface of the ferromagnetic rotor at different azimuthal locations of the stator fronts. The magnetic induction on the surface of the rotor sections covered by the corresponding stator magnetic cores is 0.6 T. The magnetic field induction levels on the outer surface of the SEMC rotor in the intermodule zone are much lower and are in the range of 0.2-0.35 T.

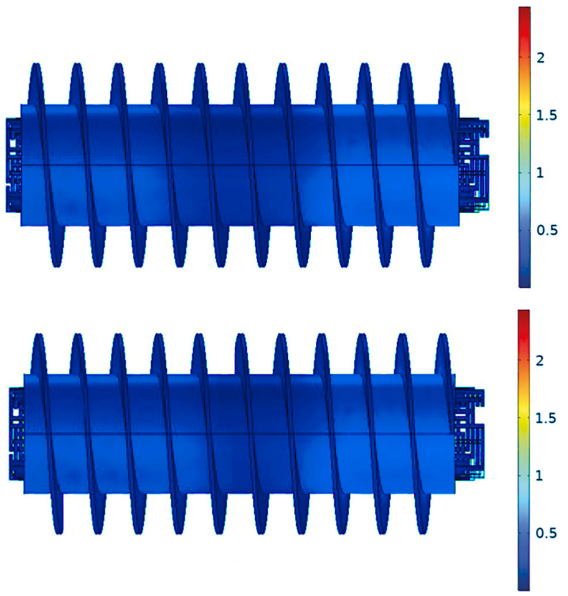

a)

b)

Figure 6. Three-dimensional image of the magnetic field induction distribution on the rotor surface with different azimuthal arrangements of the stator frontal parts

Note: scale dimension – T; a) – arbitrary azimuthal location of the frontal parts of adjacent stators; b) – magnetic fluxes of the frontal parts of adjacent stators coordinated in space and time

Source: compiled by the authors

At the same time, the length of the section with this level of magnetic induction is half as long for the variant of the magnetic fluxes of the frontal parts of adjacent stators coordinated in space and time compared to the variant of the arbitrary azimuthal arrangement of the frontal parts of adjacent stators. This indicates that the coordination in space and time of the magnetic fluxes of the frontal parts of adjacent stators creates conditions for the formation of a variable magnetic flux along the steel rotor cylinder (Fig. 1) and, accordingly, the excitation of eddy currents in the intermodule zone. It is necessary to determine the regularity of changes in the intensity of the electric and magnetic fields along the rotor cross-section, in which the outer surface has a lateral branch corresponding to the screw turn cross-section. The position of this branch changes no more than the screw turn pitch, making one revolution around the rotor circumference. Following Figure 7, the electromagnetic wave propagates perpendicular to the hollow rotor surface between the outer and inner surfaces in the intermodule zone. In the same direction, through the inner and outer surfaces, energy flows into the rotor array, which is given by the Poynting vector $\bar{P}$, caused by the electric and magnetic field components perpendicular to it and tangent to the surface.

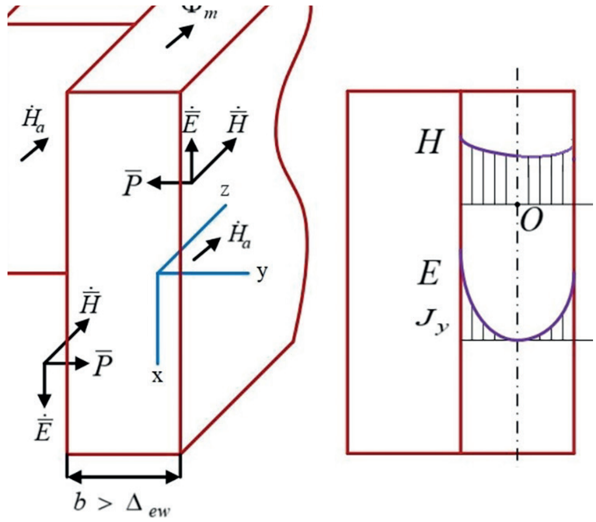

Figure 7. Distribution of electromagnetic field components and density of eddy currents in the array of the intermodule zone of the SEMC rotor

Note: $\dot{E}$ i $\dot{H}$ – amplitude values of the electric and magnetic field intensity vectors, respectively; H_a – axial component of the magnetic field strength; $\bar{P}$ – Poynting vector; $\dot{\Phi}_m$ – magnetic flux; b – rotor thickness; Δ_{ew} – electromagnetic wave penetration depth; J_y – eddy current density along the rotor thickness

Source: compiled by the authors

The electric field causes conduction current and heating of the rotor mass, and the field amplitudes decay as the electromagnetic wave propagates deeper into the metal. The final conductivity of the rotor causes the presence of a tangential component of the electric field E_τ when current flows on its surface. The electric field strength and eddy current density decrease according to the law:

$$j(y) = \gamma E_\tau(y) = \gamma E_\tau(y) exp(-a_j y), \qquad (2)$$

where a_j – wave propagation constant.

The amplitude values of the electric $\dot{E}$ and magnetic $\dot{H}$ field intensity vectors, as well as the wave propagation constant a_j, will be different when the wave penetrates the boundaries of the hollow rotor surfaces in the presence of a lateral branch in the form of ribs on the outer surface of the rotor. The temperature distribution T is determined as a solution to the equation as follows:

$$\lambda \Delta T - c\rho \frac{\partial T}{\partial t} = -Q, \quad (3)$$

where λ, c, p – respectively thermal conductivity, heat capacity and density of the material; Q – specific heat emissions. The heat emission in the rotor array is calculated by the formula:

$$Q = {J_z^2}/{\gamma(T)}, \quad (4)$$

where the electrical conductivity of the rotor iron at each point depends on the temperature T. For a two-dimensional modelling problem, equation (3) is presented in the following form:

$$\lambda \frac{\partial^2 T}{\partial x^2} + \lambda \frac{\partial^2 T}{\partial y^2} - c\rho \frac{\partial T}{\partial t} = Q. \quad (5)$$

The interconnection of electromagnetic and thermal processes is manifested in the mutual influence of temperature, electrical conductivity, eddy current density and specific heat emissions, which is reflected in formulas (3-4). Boundary and initial conditions are set for equation (5). When constructing the mathematical model, it was assumed that the main heat transfer from the rotor to the bulk material was carried out in the form of heat flow through the outer surface G (Fig. 1). This assumption is met by the second-order boundary condition, which sets the average value of the heat flux at the boundary of the computational domain:

$$q|_G = \frac{1}{R_{2H}} \int_{S'} Q ds = \frac{1}{R_{2H}} \int_{S'} \left[{J_z^2}/{(\gamma)T} \right] ds, \quad (6)$$

where R_{2H} – outer rotor radius; S' – outer radius of the rotor area of integration. Expression (6) also determines the relationship between the electromagnetic and thermal tasks.

The study considers the effect of temperature on the nature of electromagnetic processes. Approximately, the process of penetration of an electromagnetic field wave into the rotor array along the y-coordinate with a harmonically varying magnetic flux in time can be represented by the following expression:

$$J(y) = J_{m^{e^{-ky}}}, \quad (7)$$

where $k = \sqrt{\omega\mu/2\rho}$; ω is the angular frequency of the field change; μ is the magnetic permeability; ρ is the resistivity, which varies with temperature according to the known law $\rho = \rho_0[1 + \alpha(T - T_0)]$, where ρ_0 is the resistivity at temperature T_0. The dependence of the magnetic permeability of steel on temperature is more complex and is determined by empirical dependencies. The differential equation for determining the temperature increase of the surface of a ferromagnetic rotor and the corresponding temperature increase of the medium $\Delta T_{en.m}$ is as follows:

$$R_r \frac{d(\Delta T_r)}{dt} + \Delta T_r = \Delta T_{en.m}, \quad (8)$$

where R_r is the thermal time constant of the rotor design zone; $\Delta T_{en.m}$ is the temperature increase of the medium; ΔT_r is the temperature increase of the rotor. The thermal time constant of a ferromagnetic rotor:

$$R_r = \frac{m_r c_r}{2 \cdot G_{TCR}}, \quad (9)$$

where m_r, c_r – mass and specific heat capacity of the rotor material, respectively; G_{TCR} – rotor thermal conductivity. The thermal conductivity G_{TCR} is calculated for a homogeneous cylindrical wall with heat sources and heat dissipation through the outer wall, considering the helical rotor blades (fins):

$$G_{TCR} = \frac{2\pi \cdot r^2 \cdot l_r}{\frac{1}{\alpha_1} + \frac{r_2 - r_1}{\lambda} + \frac{1}{\alpha_2[1 + A_{0S}(k_{0S} - 1)]}}, \quad (10)$$

where l_r – rotor length; r_1, r_2 – inner and outer radii of the cylindrical rotor, respectively; λ – thermal conductivity of the rotor material; α_1, α_2 – are, respectively, the heat transfer coefficient on the un-finned surface of the rotor wall and the finned surface of the rotor; A_{0S} – finning efficiency factor; k_{0S} – the coefficient of finning of the rotor surface, equal to the ratio of the total area of the finned surface to the area of the smooth rotor surface. The proposed method for calculating the magnetic field and thermal parameters is advisable to implement for an end-arc squirrel-cage induction motor with an electrically conductive rotor. Unlike the method used by A.P. Rashchepkin *et al.* (2017), the modularity of the rotor design and the combination of the rotor with the working body were considered.

The rotor of the SEMC performs the functions of an actuator and is used as a direct drive, in which a wide range of rotational speeds can be formed without a semiconductor converter. Similar results were achieved in the works of P.J. Holik *et al.* (2007), and B. Virlan *et al.* (2013), which present a comprehensive study of the performance of an induction motor (IM) with an external rotor and a multi-pole stator winding.

In recent years, a large number of studies have focused on methods to improve the energy efficiency of SRIM. In comparison with the results of V.M. Sundaram *et al.* (2015), and M.V. Cistelecan *et al.* (2010), the proposed design, modelling, and experimental studies of the SEMC provide comparable performance at high slip in terms of average/pulsating torque with a significant reduction in the total copper consumption, considering the spatial harmonics of the magnetomotive force in the air gap, including saturation effects.

The magnetic field created on the outer surface of the rotor must be rotating. Therefore, this effect can be considered as a kind of electromagnetic stirrer (Zablodskiy *et al.*, 2021). In the case of using such a field, for example, in liquid media, eddy currents arise that create their magnetic field and interact with the rotating stator field, which contributes to more intense heat and mass transfer in the liquid (Smith, 2015).

Figure 8 shows thermograms of the outer surface of the rotor of the SEMC prototype with an arbitrary azimuthal arrangement of the fronts of adjacent stators and with the magnetic fluxes of the fronts of adjacent stators coordinated in space and time.

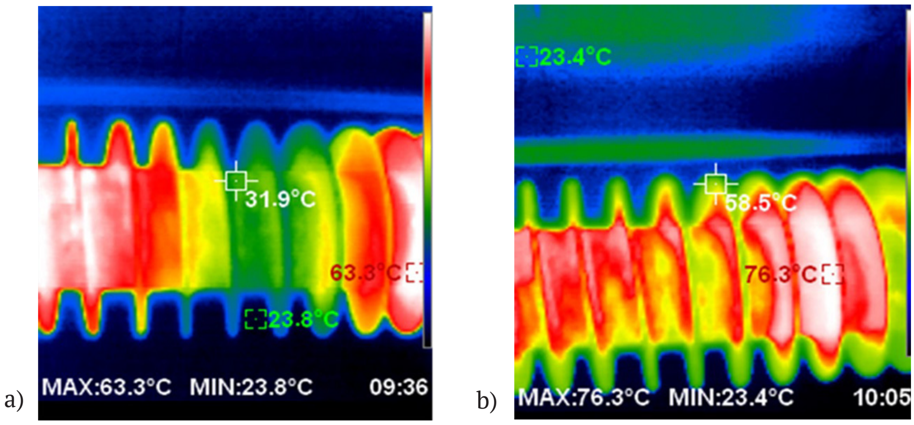

Figure 8. Thermogram of the outer surface of the rotor of the prototype SEMC
Note: the thermograms were recorded after 7 minutes of operation in the short-circuit mode at a voltage of U = 73V. 2; a) prototype with an arbitrary azimuthal arrangement of the frontal parts of adjacent stators; b) prototype with magnetic fluxes of the frontal parts of adjacent stators coordinated in space and time
Source: compiled by the authors

It is noticeable that in the case of magnetic fluxes of the frontal parts of adjacent stators coordinated in space and time, a certain uniformity of temperature field distribution along the rotor length, including the intermodule zone, is achieved. Figure 9 shows the distribution of current density (z-component) in the cross-section of the SEMC module. The eddy currents are concentrated at the penetration depth from the rotor inner surface, with the current penetration depth $\Delta = 1/k$ depending on the thermal state and sliding mode of the SEMC:

$$\Delta = \sqrt{2\rho_0[1 + \alpha(T - T_0)]/\omega\mu}. \quad (11)$$

In contrast to C. Wengerkievicz *et al.* (2022), who acquired results using two-dimensional finite element modelling, our work considers the regime of large slips up to 80%. The difference in the distribution of eddy currents at slips close to the idle stroke and slips corresponding to the full screw loading regime was noted. The magnetic permeability μ of the rotor material is not constant, so its magnetic saturation is considered. For structural carbon steels, the values are in the range of strong fields (H = $2 \cdot 10^{-3}$-$12 \cdot 10^{-3}$ A/m) have slight fluctuations when heated to temperature 400°C, and then begin to decrease, reaching unity at the Curie point temperature.

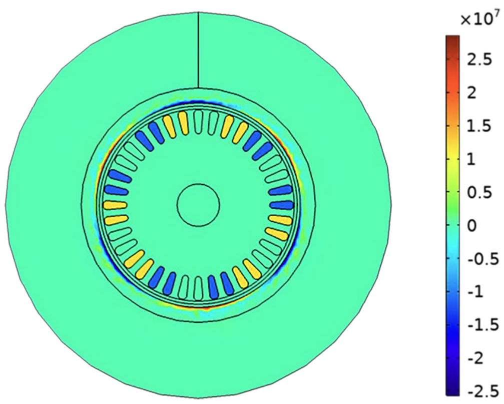

Figure 9. Distribution of current density (z-component) in the cross-section of the SEMC module, A/m^2
Source: compiled by the authors

The determination of the current density distribution in the end regions is problematic due to the lack of special methods and models. The method proposed by M. Jagiela *et al.* (2012), which is based on the numerical determination of the dimensionless rotor end coefficient using a combination of three-dimensional and two-dimensional finite element models, was developed for high-speed induction motors with a solid rotor and does not consider the operation of an electromagnetic system with several stators and a common rotor. To form an analytical method for calculating the magnetic field and electromagnetic field energy distribution in the intermodule space of the SEMC, it may be advisable to use Maxwell's system of equations for the quasi-stationary regime and integral transformations into Fourier series along the azimuthal coordinate (Rashchepkin *et al.*, 2017).

The distinctive feature of the SEMC is the conversion of the concept of "power losses", which are determined by standard loss allocation procedures, for example, for induction motors, into the concept of "dissipative energy component". In the SEMC, all types of dissipative energy (electrical and magnetic) are attributed to useful (in this case, thermal) energy. Figure 10 shows the distribution of electrical energy density for the cross-section of a SEMC module.

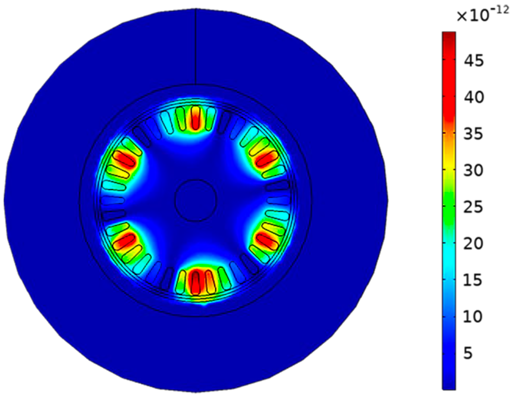

Figure 10. Electric energy density for the cross-section of the SEMC module, J/m^3
Source: compiled by the authors

It can be seen that the main electrical energy consumed is distributed in the stator tooth zone and the zone of electromagnetic field penetration into the rotor. The methods of loss segregation proved to be appropriate by tests with a locked rotor and no load, which was used by C. Mellak *et al.* (2022) in experimental studies of induction motors with smooth solid rotors. Table 1 shows the experimental data of the prototype of the SEMC. Magnetic induction, electric field intensity, and electromagnetic radiation flux density were measured in the short-circuit mode at the minimum possible distance of 1 mm from the rotor surface of the SEMC.

Table 1. Experimental data of the prototype sample of the SEMC

Measurement area	Parameters			
	Magnetic induction, mT	Electric field strength, V/m	Density of electromagnetic radiation flux, mW/m^2	Temperature, (Fig. 3)
1	60	0.03	0.7	48
2	100	0.03	0.9	51
3	170	0.03	1.8	62
4	400	0.2	523	74
5	380	0.15	520	76.2
6	410	0.15	525	76.3

Note: the temperature distribution is given for the variant with the magnetic fluxes of the frontal parts of adjacent stators coordinated in space and time
Source: compiled by the authors

A. Wasak *et al.* (2019) noted that a rotating magnetic field is used as a tool to improve the properties of enzymes. At the interfaces of matter, the Hall effect in the presence of a magnetic field promotes intense interaction of the electric fields of bulk ion charges and electric charges of the interface. Therefore, it was important to determine the distribution of the normal component of the electric field strength for the cross-section of the SEMC module, especially on the rotor's outer surface. Figure 11 shows the distribution of the normal component of the electric field intensity for the cross-section of the SEMC module.

The electric field intensity on the rotor's outer surface reaches 0.8 V/m in the areas corresponding to the location of the stator crowns and depends on the current activity of the phases at the moment. Thus, the control of the rotor thermal and speed regime makes it possible to create conditions for bioenergy stimulation on its surface in places of contact with the medium or to maintain the process of its electrode heating.

Considering the objective reason for the remote location of the device sensors, we extrapolated the data for measuring magnetic induction, electric field strength, and electromagnetic radiation flux density of the SEMC prototype. The adequacy of the mathematical models proposed for the numerical modelling of the experimental data of the SEMC prototype was confirmed (Table 1). The deviations do not exceed 9.5%. Based on the results of the simulation, Figure 12 shows the distribution of electromagnetic forces acting in the air gap of the SEMC.

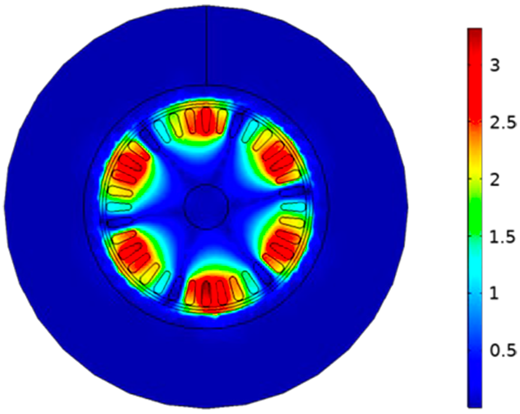

Figure 11. Distribution of the normal component of the electric field intensity for the cross-section of the SEMC module, V/m³

Source: compiled by the authors

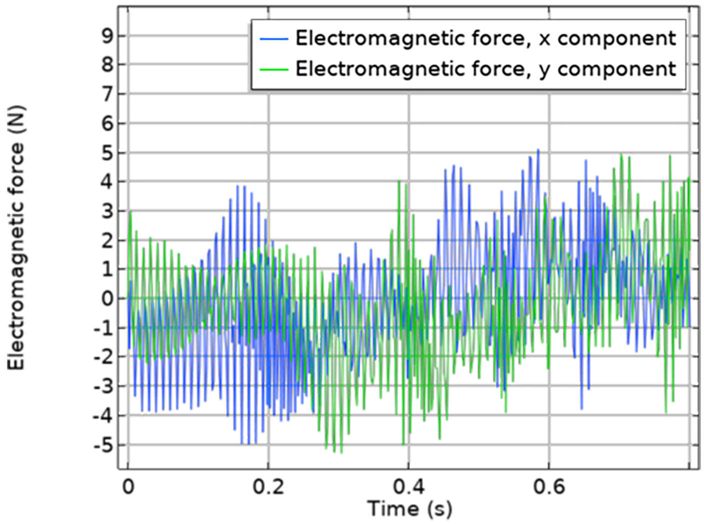

Figure 12. Distribution of electromagnetic forces

Source: compiled by the authors

The frequency range of electromagnetic forces is 90-120 Hz and significantly exceeds the frequency of the stator supply current. The data of the study by V. Bulgakov *et al*. (2020) also indicate that under the influence of vibration, materials undergo transformations whose properties depend on the vibration intensity, and, for example, keratin materials go into a state of fluidisation. In addition, the determination of the distribution of electromagnetic forces and, accordingly, electromagnetic moments allow, in comparison with the calculations of P. Singha & K. Muthukumarappan (2016) to improve the accuracy of estimating the effect of hydrolysis parameters on the mixing torque for single- and twin-screw electromechanical converters.

The found regularities of the distribution of surface parameters and characteristics of the electromagnetic field of the SEMC are confirmed by the results of the study by T.Y. Chen *et al.* (2017) create the basic conditions for the formation of the necessary modes of processing substances, substrates and the technological environment. A certain part of biopolymers does not have a strictly ordered crystal structure but has a dissipative fractal structure or a certain level of relative order, for example, the paramagnetic downy mass of birds. High molecular weight compounds, such as lignins and their substrates, have a structure of several interconnected levels.

The regularities of the distribution of eddy currents and components, of the electromagnetic field under variations in the length of the intermodule zone and the parameters of the helical winding require careful study. However, consideration of real processes of electromagnetic interaction with the medium, which include not only the processing of the technological environment utilizing electromagnetic disturbances, but also the processes of destruction of its structure, generation of its electromagnetic oscillations, and ion exchange, can be demonstrated in future work on metrologically and hardware-improved laboratory samples.

CONCLUSIONS

Using the proposed research methodology and the results of modelling and experimental studies, it was confirmed that the screw-type electromechanical converter can be considered as a source of multiphysical influence on the environment in the formation of technological operations for the processing of substances and technogenic waste. Depending on the loading mode of the SEMC, the technological environment can be represented in the following types: at idle (system warm-up mode) – air; at the main operating mode – a continuous heterogeneous environment using averaged characteristics (specific conductivity, magnetic and dielectric constant).

To consider the properties of the technological environment, it is proposed to introduce into the mathematical model vectors of electric induction and magnetic field intensity, which are different in content, and consider all the above currents, namely: eddy current; polarisation current of bound charges; free carrier current. To form an algorithm for the multiphysical influence on the technological environment, namely, the uniform distribution along the rotor surface of temperature, pressure, magnetic induction, and electric field strength, a method based on the numerical determination of the transverse and longitudinal edge effect of a common rotor for two stators of a SEMC using a combination of three-dimensional and two-dimensional finite element models is proposed. The regularities of the magnetic induction distribution on the outer surface of a ferromagnetic rotor at different azimuthal locations of the stator frontal parts are established. In the case of coordinated space and time magnetic fluxes of the frontal parts of adjacent stators, a certain uniformity of the temperature field distribution along the rotor length, including the intermodule zone, is achieved.

The electric field intensity on the rotor's outer surface reaches 0.8 V/m in areas corresponding to the location of the stator tooth crowns and depends on the current activity of the phases at the moment. Controlling the thermal and speed regime of the rotor makes it possible to create conditions for bioenergy stimulation on its surface in places of contact with the medium or to support the process of electrode heating of the technological medium. Further research will be devoted to the development of designs and control systems for industrial models of screw electromechanical units and energy-saving technologies based on them.

ACKNOWLEDGEMENTS

This work was supported by the Ministry of Education and Science of Ukraine (№ 0123U102165).

CONFLICT OF INTEREST

The authors declare no conflict of interest.

REFERENCES

[1] AC/DC module user's guide, COMSOL Inc. (2018). Retrieved from https://doc.comsol.com/5.4/doc/com.comsol.help.acdc/ACDCModuleUsersGuide.pdf.

[2] Bulgakov, V., Sevostianov, I., Kaletnik, G., Babyn, I., Ivanovs, S., Holovach, I., & Ihnatiev, Y. (2020). Theoretical studies of the vibration process of the dryer for waste of food. *Rural Sustainability Research*, 44(339), 32-45. doi: 10.2478/plua-2020-0015.

[3] Campuzano, F., Brown, C.R., & Martínez, J.D. (2019). Auger reactors for pyrolysis of biomass and wastes. *Renewable and Sustainable Energy Reviews*, 102, 372-409. doi: 10.1016/j.rser.2018.12.014.

[4] Chen, T.Y., Wang, B., Wu, Y.Y., Wen, J.L., Liu, C.F., Yuan, T.Q., & Sun, R.C. (2017). Structural variations of lignin macromolecule from different growth years of Triploid of *Populus tomentosa* Carr. *International Journal of Biological Macromolecules*, 101, 747-757. doi: 10.1016/j.ijbiomac.2017.03.146.

[5] Cistelecan, M.V., Ferreira, F.J., & Popescu, M. (2010). Three phase tooth-concentrated multiple-layer fractional windings with low space harmonic content. In *2010 IEEE Energy Conversion Congress and Exposition* (pp. 1399-1405). Atlanta: IEEE. doi: 10.1109/ECCE.2010.5618267.

[6] Feng, C., Li, Z., Wang, Z., Wang, B., & Wang, Z. (2019). Optimizing torque rheometry parameters for assessing the rheological characteristics and extrusion processability of wood plastic composites. *Journal of Thermoplastic Composite Materials*, 32(1), 123-140. doi: 10.1177/0892705717744828.

[7] Holik, P.J., Dorrell, D.G., & Popescu, M. (2007). Performance improvement of an external-rotor split-phase induction motor for low-cost drive applications using external rotor can. *IEEE Transactions on Magnetics*, 43(6), 2549-2551. doi: 10.1109/TMAG.2007.893304.

[8] Jagiela, M., & Garbiec, T. (2012). Determination of best rotor length in solid-rotor induction motor with axial slitting. *Archives of Electrical Engineering*, 61(2), 267-276. doi: 10.2478/v10171-012-0022-2.

[9] Kaplun, V., Makarevych, S., & Chuenko, R. (2022). Modelling of asynchronous motor with split stator windings on the principle of a rotary autotransformer. *Przeglad Elektrotechniczny*, 98(3). doi: 10.15199/48.2022.03.10.

[10] Laidoudi, A., Duchesne, S., Morganti, F., & Velu, G. (2020). High-power density induction machines with increased windings temperature. *Open Physics*, 18(1), 642-651. doi: 10.1515/phys-2020-0131.

[11] Mazlan, M.M., Talib, R.A., Mail, N.F., Taip, F.S., Chin. N.L., Sulaiman, R., Shukri, R., & Mohd Nor, M.Z. (2019). Effects of extrusion variables on corn-mango peel extrudates properties, torque and moisture loss. *International Journal of Food Properties*, 22, 54-70. doi: 10.1080/10942912.2019.1568458.

[12] Mellak, C., Deuringer, J., & Muetze, A. (2022). Impact of aspect ratios of solid rotor, large air gap induction motors on run-up time and energy input. *IEEE Transactions on Industry Applications*, 58(5), 6045-6056. doi: 10.1109/TIA.2022.3180030.
[13] Mushtruk, M., Gudzenko, M., Palamarchuk, I., Vasyliv, V., Slobodyanyuk, N., Kuts, A., Nychyk, O., Salavor, O., & Bober, A. (2020). Mathematical modeling of the oil extrusion process with pre-grinding of raw materials in a twin-screw extruder. *Potravinarstvo Slovak Journal of Food Sciences*, 14, 937-944. doi: 10.5219/1436.
[14] Rashchepkin, A.P., Karlov, O.M., & Kryshchuk, R.S. (2017). Structure of magnetic field of the axial arc-stator induction motor with solid bimetallic disc rotor. *Proceedings of the Institute of Electrodynamics of the National Academy of Sciences of Ukraine*, 47, 28-36.
[15] Singha, P., & Muthukumarappan, K. (2016). Effects of processing conditions on the system parameters during single screw extrusion of blend containing apple pomace. *Journal of Food Process Engineering*, 40(4), 1-11. doi: 10.1111/jfpe.12513.
[16] Smith, C.W. (2015). Electromagnetic and magnetic vector potential bio-information and water. *Homeopathy*, 104(4), 301-304. doi: 10.1016/j.homp.2015.08.006.
[17] Sundaram, V.M., & Toliyat, H.A. (2015). A fractional slot concentrated winding (FSCW) configuration for outer rotor squirrel cage induction motors. In *2015 IEEE International Electric Machines & Drives Conference* (pp. 20-26). USA: IEEE. doi: 10.1109/IEMDC.2015.7409031.
[18] Virlan, B., Benelghali, S., Simion, A., Livadaru, L., Outbib, R., & Munteanu, A. (2013). Induction motor with outer rotor and ring stator winding for multispeed applications. *IEEE Transactions on Energy Conversion*, 28(4), 999-1007. doi: 10.1109/tec.2013.2279841.
[19] Wasak, A., Drozd, R., Jankowiak, D., & Rakoczy, R. (2019). Rotating magnetic field as tool for enhancing enzymes properties-laccase case study. *Scientific Reports*, 9(1), 1-9. doi: 10.1038/s41598-019-39198-y.
[20] Wengerkievicz, C.A., Batistela, N.J., Sadowski, N., Huguet, T., & Lefèvre, Y. (2022). Experimental loss segregation in a solid rotor induction motor. *Journal of Microwaves*, *Optoelectronics and Electromagnetic Applications*, 21, 584-597. doi: 10.1590/2179-10742022v21i4268098.
[21] Wolnik, T., & Jarek, T. (2022). Solid rotor core vs. lamination rotor core in fractional-slot pmsm motor with high power density. *Energies*, 15(15), article number 5729. doi: 10.3390/en15155729.
[22] Zablodskiy, N., Chuenko, R., Gritsyuk, V., Kovalchuk, S., & Romanenko, O. (2021). The numerical analysis of electromechanical characteristics of twin-screw electromechanical hydrolyzer. *In 2021 11th International Conference on Advanced Computer Information Technologies (ACIT)* (pp. 130-135). Deggendorf: IEEE. doi: 10.1109/ACIT52158.2021.9548392.
[23] Zablodskiy, N., Pliugin, V., & Gritsyuk, V. (2014). Submersible electromechanical transformers for energy efficient technologies of oil extraction. In *Progressive technologies of coal, coaled methane, and ores mining* (pp. 223-227). Boca Raton: CRC Press.

Стефан Юнге

Доктор технічних наук, професор
Берлінський університет прикладних наук
13353, вул. Люксембурзька, 10, м. Берлін, Німеччина
https://orcid.org/0000-0002-8045-4103

Микола Миколайович Заблодський

Доктор технічних наук, професор
Національний університет біоресурсів і природокористування України
03041, вул. Героїв Оборони, 15, м. Київ, Україна
https://orcid.org/0000-0001-8889-8158

Наталія Анатоліївна Заєць

Доктор технічних наук, професор
Національний університет біоресурсів і природокористування України
03041, вул. Героїв Оборони, 15, м. Київ, Україна
https://orcid.org/0000-0001-5219-2081

Роман Миколайович Чуєнко

Кандидат технічних наук, доцент
Національний університет біоресурсів і природокористування України
03041, вул. Героїв Оборони, 15, м. Київ, Україна
https://orcid.org/0000-0002-9339-9764

Станіслав Ігорович Ковальчук

Аспірант
Національний університет біоресурсів і природокористування України
03041, вул. Героїв Оборони, 15, м. Київ, Україна
https://orcid.org/0000-0002-1194-3464

Електромеханічний перетворювач шнекового типу як джерело мультифізичного впливу на технологічне середовище

Анотація. При забезпечення надійності роботи електромеханічних перетворювачів у важких умовах, виникає проблема підвищення енергоефективності їх застосування шляхом структурної, функціональної і теплової інтеграції з технологічним середовищем. Тому метою дослідження було визначення умов безпосереднього мультифізичного впливу електромеханічного перетворювача шнекового типу на технологічне середовище. Застосовано метод, який заснований на чисельному визначенні в програмному середовищі Comsol Multiphysics характеристик шнекових електромеханічних перетворювачів з використанням комбінації тривимірних і двовимірних моделей кінцевих елементів, обмежених ротором з внесенням лопатей до розрахункової області. Досліджувались два варіанта формування алгоритму мультифізичного впливу на технологічне середовище: локальна концентрація впливу на певних ділянках ротора і рівномірний розподіл вздовж поверхні ротора температури, тиску, магнітної індукції, напруженості електричного поля. Встановлені закономірності розподілу магнітної індукції на зовнішній поверхні феромагнітного ротора при різному азимутальному розташуванні лобових частин суміжних статорів. Визначено розподіл нормальної складової щільністі магнітного потоку при наявності контакта з технологічним середовищем у вигляді рутілового продукту або ільменітового концентрату. Споживана електрична енергія розподілена в зубцевій зоні статора та зоні проникнення електромагнітного поля в ротор. Вихрові струми сконцентровані на глибині проникнення від внутрішньої поверхні ротора, при цьому глибина проникнення залежить від теплового стану та режиму ковзання. Напруженість електричного поля на зовішній поверхні ротора досягає 0,8 V/m на відповідних до розташування коронок зубців статора ділянках і залежить від струмової активності фаз в даний момент. Регулювання температурного та швидкісного режиму ротора дає можливість на його поверхні в місцях контакту з середовищем створювати умови біоенергетичної стимуляції або підтримувати процес низькоамперного електролізу імпульсами невисокої напруги в тонкому шарі. Підтверджена адекватність математичних моделей, які були запропоновані для чисельного моделювання, експериментальним даним макетного зразка шнекового електромеханічного перетворювача, відхилення не перевищують 9,5%. Отримані результати дозволяють прогнозувати оптимальні показники електромагнітних та теплообмінних процесів у шнекових електромеханічних перетворювачах, пов'язаних з технологічним середовищем

Ключові слова: магнітна індукція; вихрові струми; температурне поле; електромагнітне поле; термограма; магнітна проникність